

Spatial-temporal Vehicle Re-identification

Hye-Geun Kim¹, YouKyoung Na², Hae-Won Joe², Yong-Hyuk Moon^{3,4}, Yeong-Jun Cho¹

¹Department of Artificial Intelligence Convergence, Chonnam National University

²Department of Artificial Intelligence, Chonnam National University

³Electronics and Telecommunications Research Institute

⁴Department of AI, University of Science and Technology

¹{hyegeunkim, yj.cho}@jnu.ac.kr ²{me6zero, 214583}@jnu.ac.kr ^{3,4}yhmoon@etri.re.kr

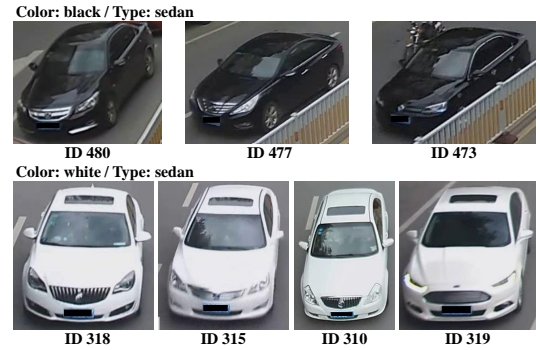
Abstract

Vehicle re-identification (ReID) in a large-scale camera network is important in public safety, traffic control, and security. However, due to the appearance ambiguities of vehicle, the previous appearance-based ReID methods often fail to track vehicle across multiple cameras. To overcome the challenge, we propose a spatial-temporal vehicle ReID framework that estimates reliable camera network topology based on the adaptive Parzen window method and optimally combines the appearance and spatial-temporal similarities through the fusion network. Based on the proposed methods, we performed superior performance on the public dataset (VeRi 776) by 99.64% of rank-1 accuracy. The experimental results support that utilizing spatial and temporal information for ReID can leverage the accuracy of appearance-based methods and effectively deal with appearance ambiguities.

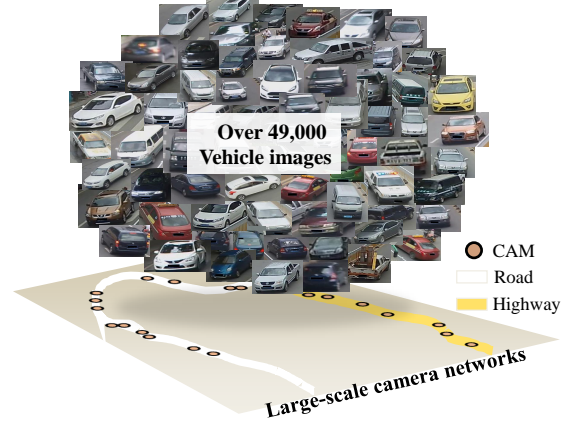
1. Introduction

Recently, a large number of surveillance cameras have been installed in public places for safety, traffic monitoring, and security. However, monitoring all the cameras requires lots of human effort and resources. To reduce the human efforts, re-identification (ReID) that automatically tracks targets across non-overlapping multiple cameras can be utilized. Especially in traffic surveillance systems, vehicle ReID is essential due to the rapid flow of many vehicles on the scene.

In general, most studies have focused on targets' visual appearances to perform ReID. For example, many studies [1, 5] have proposed feature learning methods to represent appearances of targets. Similarly, metric learning methods [21, 37] also have been proposed to measure feature distances between query and gallery images effectively. Recently, developments in deep learning have led to higher



(a) Appearance ambiguity problem in vehicle ReID



(b) High computational complexity

Figure 1. Challenges in vehicle re-identification

performance improvements by training both visual features and distance metrics [9, 11]. Those appearance-based methods are robust to target pose variations, viewpoints changes, and illumination changes.

However, compared to person, vehicles have different characteristics leading to new challenges in re-identification. First, vehicles with exactly the same appear-

ances make high appearance ambiguities (Fig. 1 (a)). People show distinctive features, such as different faces, clothing, and body shapes, whereas many vehicles have the same appearance features due to the same model types. Second, appearing a very large number of vehicles in multiple cameras occurs both high computational complexity and low identification performance (Fig. 1 (b)). Relying only on the target appearances is not effective for the vehicle ReID problem.

To alleviate the appearance ambiguity, ReID studies that use additional spatial and temporal information have been proposed [7, 31, 35]. They built a camera network topology explaining spatial and temporal relationships between cameras and utilized the topology to reduce redundant searching time ranges of queries. While the methods exhibit potential for improving appearance-based ReID models [9, 11], they still have limitations. The camera network topology modeling approaches are simple, and the integration of the appearance model with spatio-temporal information lacks optimization.

In this work, we propose a spatial-temporal vehicle ReID framework to overcome the limitations. The proposed ReID framework consists of two main parts: 1) camera network topology estimation, 2) fusing appearance similarity and spatial-temporal probabilities. For the camera network topology estimation, we propose an adaptive Parzen window that is robust to outliers and sparse responses between camera pairs (Sec. 4.1). It can effectively handle different connection strengths of camera pairs for reliable camera network topology estimation. After estimating the topology, we train a fusion network (fusionNet) that can optimally combine appearance similarity and spatial-temporal probabilities (Sec. 4.2). To evaluate the proposed methods, we tested VeRi776 [23] vehicle ReID dataset. In the experiments, we validated the effectiveness of our proposed methods. Our methods performed the best vehicle ReID performances by 99.34% of rank-1 accuracy and 92.40% of mAP score compared to state-of-the-art methods.

The main contributions of this work are as follows:

- We estimated a reliable camera network topology based on the proposed adaptive Parzen window.
- We trained a fusion network to optimally combine two different similarities (appearance and spatial-temporal).
- We achieved superior performance (99.64% of rank-1 accuracy) in the vehicle ReID task.

To the best of our knowledge, this is the first attempt to train a network for fusing appearance and spatial-temporal similarities. In addition, the flexibility of the proposed framework is high because any kind of appearance-based model can be used as a baseline.

2. Related Works

2.1. Appearance-based ReID

Most re-identification (ReID) studies have focused on learning visual representations of images to distinguish their appearances. To this end, feature learning and metric learning methods have been widely studied. For the feature learning method, Ahmed *et al.* [1] initially utilized deep convolutional neural networks (CNN) architecture that captures local relationships between two input images based on mid-level features. Chen *et al.* [5] improved the CNN-based ReID and proposed a Deep Pyramid Feature Learning (DPFL) CNN, which can learn scale-specific discriminative features. Similarly, the studies [6, 30] tried to extract robust local features. To capture more details of appearances, Khamis *et al.* [18] utilized attributes of targets for ReID. Huynh *et al.* [17] also used multi-head with attention mechanism to improve visual representation quality. Recently, He *et al.* [13] proposed TransReID, which is the first attempt to utilize a transformer to learn robust features from the image patches. For a better visual representation, Li *et al.* [22] proposed CLIP-ReID, which fine-tunes the initialized visual model by the image encoder in CLIP.

For metric learning, learning the Mahalanobis distance [21, 37] has been widely studied. Especially, optimizing triplet loss for deep metric learning [6, 11, 14] has shown superior performances in ReID tasks. To alleviate the negative effect of intra-class variance and inter-class similarity, Bai *et al.* [2] utilized inter-class triplet embedding and intra-class triplet embedding. Ghosh *et al.* [9] proposed Relation Preserving Triplet Mining (RPTM), a feature matching guided triplet mining scheme that ensures that triplets preserve natural subgroupings in object IDs. Meanwhile, several methods [8, 27, 32] utilized additional cues such as human pose and body parts to handle pose variations and occlusions problems in ReID. However, relying only on appearance for ReID is still hard to alleviate appearance ambiguity.

2.2. Spatial-temporal ReID

To overcome the limitations of the appearance-based ReID, many studies have utilized spatial-temporal information of cameras and target objects. In general, they employed appearance-based ReID model as their baseline, and additionally exploited the spatial and temporal information. In spatial-temporal ReID, there are two main issues: 1) Estimating spatial-temporal information so-called camera network topology in given camera networks. 2) Utilizing the estimated camera network topology for ReID.

To estimate the camera network topology, studies [7, 15, 35] have tried to design accurate transition time distributions of targets (e.g., human, vehicle). For example, Huang *et al.* [15] utilized the Weibull distribution to for-

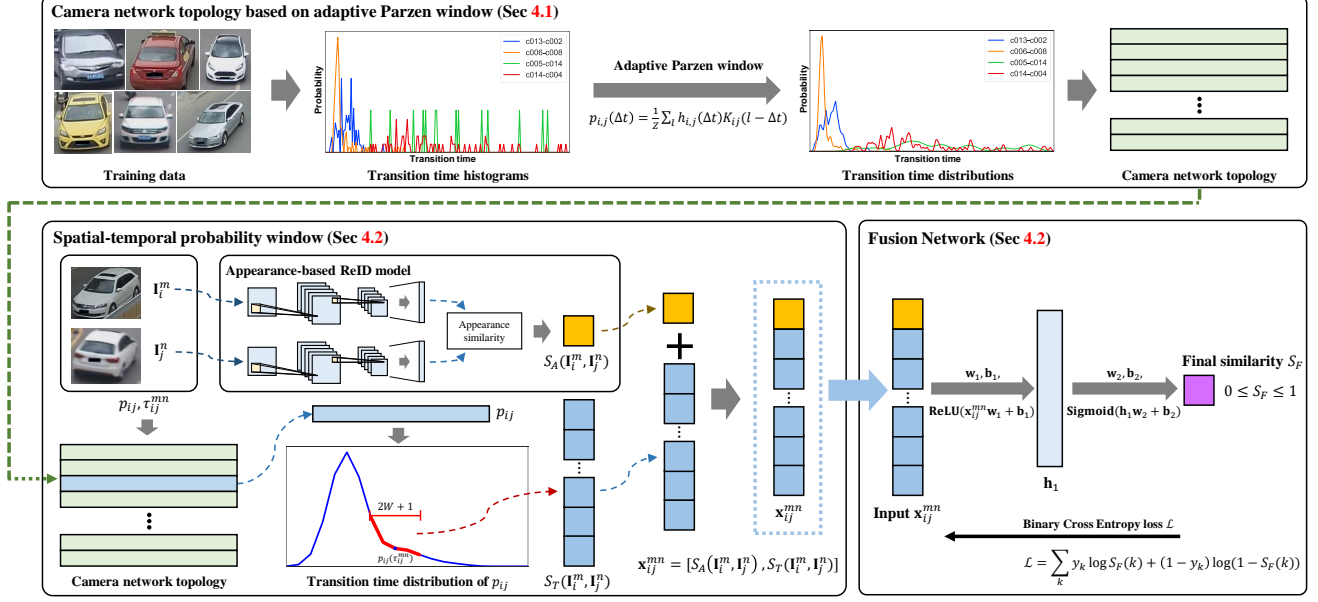


Figure 2. The overall framework for vehicle re-identification with spatial-temporal information

mulate the pedestrian transition probability. Cho *et al.* [7] proposed joint estimations of camera network topology and person ReID. Wang *et al.* [35] proposed the Histogram-Parzen to estimate spatial-temporal probability distributions. Also, Huang *et al.* [16] modeled a spatio-temporal model leveraging by vehicle pose view embedding. Liu *et al.* [23, 24] proposed a progressive vehicle ReID that partially utilizes simple spatial-temporal information. Similarly, the studies [25, 29, 38] estimated spatial-temporal information to filter out irrelevant gallery images. Shen *et al.* [31] proposed a Siamese-CNN + Path-LSTM network to predict the path through visual feature information and spatial-temporal information.

While numerous spatial-temporal ReID methods have been proposed, there are still some limitations. First, methodologies for estimating spatial-temporal models are quite simple. For example, many methods [23–25] just built objects’ transition time distributions based on the positive responses between cameras. However, noisy and sparse responses make the estimated distributions unreliable. Second, usages of the spatial-temporal information are not optimized. E.g., the studies [16, 29, 35] just merged both probabilities (i.e., appearance and spatial-temporal) with the same importance to get the joint probability. Similarly, many methods [25, 29, 38] simply utilized spatial-temporal information to reduce the searching range or perform re-ranking the initial ReID results.

3. Motivation and Main Ideas

To handle the challenges in vehicle ReID, we analyzed the characteristics of vehicles in camera networks. First, vehicles can have exactly the same appearance (e.g., model, shape, and color) according to their model types. Second, since vehicles can only move along roads and highways, vehicle movements across cameras can be predicted. To sum up, compared to person ReID, vehicles show high appearance ambiguities and predictable movements. Therefore, relying only on appearance differences between vehicles is not effective for the vehicle ReID problem.

Based on the observations of vehicles, we additionally exploit spatial and temporal relationships between cameras called a camera network topology. As shown in Fig. 2, the proposed ReID framework consists of two main parts: 1) camera network topology estimation, 2) fusing appearance and spatial-temporal similarities. We first build the topology based on the proposed adaptive Parzen window (Sec. 4.1). We then train a fusion network that optimally combines visual similarity and the camera network topology information for the final ReID prediction (Sec. 4.2).

4. Proposed Methods

4.1. Adaptive Parzen window for camera network topology estimation

Camera network topology represents spatio-temporal relationships and connections between cameras that can be represented by a graph $G = (V, E)$. The vertices V denote

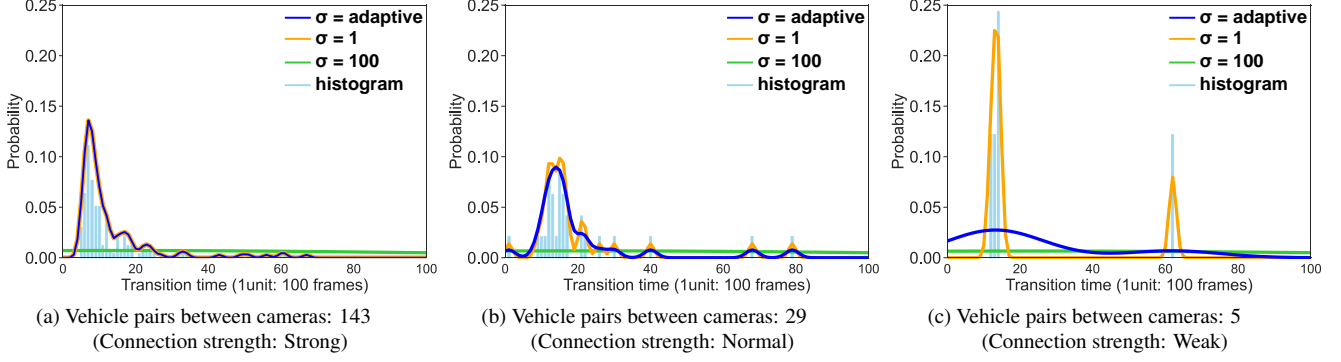


Figure 3. Examples of estimated transition time distributions between camera pairs. Each bin covers 100 frame ranges. Blue solid line (—) is the estimated distribution (p_{ij}) from the histogram (h_{ij}) by the proposed adaptive Parzen window. Best viewed in color.

cameras and the edges \mathbf{E} denote distributions of object transition time. Suppose there are N_{cam} numbers of cameras in the camera networks. Then, the topology is represented by

$$\begin{aligned} \mathbf{V} &\in \{c_i | 1 \leq i \leq N_{cam}\}, \\ \mathbf{E} &\in \{p_{ij} | 1 \leq i \leq N_{cam}, 1 \leq j \leq N_{cam}, i \neq j\}, \end{aligned} \quad (1)$$

where c denotes a camera, p_{ij} denotes an object transition time distribution between camera pairs c_i and c_j .

To build the transition time distributions p_{ij} , we used positive vehicle pairs between all camera pairs in the training dataset. Based on multiple time differences (Δt) of positive pairs, we can generate an initial histogram of the transition time $h_{ij}(\Delta t)$ as depicted in cyan lines (—) in Fig. 3. Cho *et al.* [7] proposed connectivity checking criteria whether a pair of cameras is connected or not by fitting a Gaussian model to the histogram $h_{ij}(\Delta t)$. However, this parametric method followed strong assumptions and it is hard to handle outliers and sparsity of the histogram.

Inspired by [35], a Parzen window method can be applied to the initial histograms, and we can estimate probability density function (PDF) of vehicle transition time in a non-parametric manner as follows

$$p_{ij}(\Delta t) = \frac{1}{Z} \sum_{\tau} h_{ij}(\Delta t) K(\tau - \Delta t), \quad (2)$$

where $Z = \sum_{\Delta t} h_{ij}(\Delta t)$ is a normalized factor and $K(\cdot)$ is a kernel function. For the kernel K , the work [35] used Gaussian function as

$$K(x) = \frac{1}{\sqrt{2\pi}\sigma} \exp\left(-\frac{x^2}{2\sigma^2}\right). \quad (3)$$

While the Parzen window method efficiently estimates continuous probability density functions from discrete histograms, employing a single kernel across diverse histograms from various camera pairs is not reasonable. The strength of the spatio-temporal connection between cameras can be determined by how many vehicles pass through

those cameras during a certain period of time [7]. For example, few positive pairs between two cameras indicate a weak connectivity between them. Nevertheless, the Parzen window method extremely enlarges those small responses with a small σ value as depicted in the orange line (—) in Fig 3c. In that case, it is better to use a large σ value to avoid overfitting the distribution for noise and outliers.

On the other hand, if there are lots of positive pairs between cameras, then the connectivity should be strong. However, with the large σ , the resulting distribution becomes uniform, thereby failing to capture any meaningful spatial and temporal relationships between the cameras (green line (—) in Fig. 3a). In that case, it is better to use a relatively small σ value to reflect temporal information between cameras. Thus, selecting the proper σ value is important to the estimated distribution (p_{ij}) quality.

To overcome the limitation of the original Parzen window method, we newly propose adaptive Parzen window by setting different σ_{ij} values for different camera pairs (c_i, c_j). To this end, we designed an adaptive standard deviation according to the different strength of the camera connectivity as follow

$$\sigma_{ij} = \max\left(\alpha \exp\left(\frac{-N_{ij}}{\beta}\right), 1\right), \quad (4)$$

where N_{ij} is the number of positive vehicle pairs between camera c_i and c_j . α is a positive factor that determines the maximum range of σ_{ij} . β is a smoothness factor that adjusts sensitivity of σ_{ij} . The minimum value of σ_{ij} cannot be less than 1 unit of the histogram. Then, the values of σ_{ij} lie on $[1, \alpha]$.

By considering camera indexes, Eq. 2 and Eq. 3 reformulated as

$$p_{ij}(\Delta t) = \frac{1}{Z} \sum_{\tau} h_{ij}(\Delta t) K_{ij}(\tau - \Delta t), \quad (5)$$

$$K_{ij}(x) = \frac{1}{\sqrt{2\pi}\sigma_{ij}} \exp\left(\frac{-x^2}{2\sigma_{ij}^2}\right). \quad (6)$$

As a result, we can estimate reliable distributions (p_{ij}) from the initial discrete histograms (h_{ij}) by considering the connectivity between cameras. The blue lines (—) in Fig. 3 are our results based on the adaptive Parzen window.

4.2. Fusion Network

To estimate appearance similarities between images, the proposed ReID framework can employ any appearance-based ReID method as its baseline. Images from each camera (c_i, c_j) are denoted by $\mathbf{I}_i^m, \mathbf{I}_j^n$, where m, n are indexes of the images. Then, the appearance-based ReID methods estimate the visual similarity between two images as $S_A(\mathbf{I}_i^m, \mathbf{I}_j^n)$ that lies on $[0, 1]$. Note that the proposed framework does not depend on the types of appearance-based models.

In order to perform spatial-temporal ReID, Cho *et al.* [7] used camera network topology only to restrict the searching range of the gallery. It is effective to reduce the complexity of ReID, but the spatial-temporal probability has no effect on the final similarity. On the other hand, previous studies [16, 29, 35] just merged both probabilities (i.e., appearance and spatial-temporal) with the same importance to get the joint probability. However, they neglected two points. First, the domain of each probability is not the same. Second, both appearance and spatial-temporal probabilities can be imperfect. Therefore, it is not reasonable to merge those probabilities half and half.

In this work, we optimally combines visual similarities $S_A(\mathbf{I}_i^m, \mathbf{I}_j^n)$ and estimated spatial-temporal distributions $p_{ij}(\Delta t)$ based on the fusion network. An input vector of the network for two images ($\mathbf{I}_i^m, \mathbf{I}_j^n$) in the camera pair (i, j) can be represented by

$$\mathbf{x}_{ij}^{mn} = [S_A(\mathbf{I}_i^m, \mathbf{I}_j^n), S_T(\mathbf{I}_i^m, \mathbf{I}_j^n)], \quad (7)$$

where S_A is an appearance similarity, and S_T is a spatial-temporal vector. S_T vector between images are defined by

$$S_T(\mathbf{I}_i^m, \mathbf{I}_j^n) = \left[p_{ij}(\tau_{ij}^{mn} - W), \dots, p_{ij}(\tau_{ij}^{mn} - 1), p_{ij}(\tau_{ij}^{mn}), p_{ij}(\tau_{ij}^{mn} + 1), \dots, p_{ij}(\tau_{ij}^{mn} + W) \right], \quad (8)$$

where τ_{ij}^{mn} is the time difference between two images \mathbf{I}_i^m and \mathbf{I}_j^n . W is the size of a time window. According to the W , the range of the S_T vector is determined around distributions of $p_{ij}(\tau_{ij}^{mn})$. E.g. when we set $W = 0$, the S_T becomes a scalar value as $S_T(\mathbf{I}_i^m, \mathbf{I}_j^n) = p_{ij}(\tau_{ij}^{mn})$. When we set $W > 0$, the S_T vector has a $2W + 1$ dimensional

vector. By adjusting the value of W , we can determine how much spatio-temporal information to provide for the fusion network. Then, the dimension of the input vector \mathbf{x}_{ij}^{mn} for the fusionNet is $2W + 2$.

We designed the fusion network based on simple Multi-layer Perception (MLP). We empirically found that the fusion network does not require sophisticated deep neural network structure to estimate the final similarity. The network has one hidden layer with several nodes and a one-dimensional output layer, as shown in Fig. 2. For the activation function, we used Rectified Linear Unit (ReLU) for nodes in the hidden layer, and sigmoid function for the output node. Then, the final output of the fusion network $S_F(\mathbf{I}_i^m, \mathbf{I}_j^n)$ lies on $[0, 1]$. To train the network, we optimized binary cross entropy loss defined by

$$\mathcal{L} = \sum_k y_k \log S_F(k) + (1 - y_k) \log(1 - S_F(k)), \quad (9)$$

where k is an index of training image pair, $y_k \in [0, 1]$ is the ground-truth of the k -th image pair.

5. Experimental Results

5.1. Dataset and Settings

For experiments, we used the VeRi776 [23] vehicle re-identification (ReID) dataset. It contains over 49,000 images of 776 different vehicles captured by 20 non-overlapping synchronized cameras ($N_{cam} = 20$). Each image contains vehicle ids, timestamps (frame No.), and camera ids. We used 37,778 training images from 576 vehicle identities to train the appearance-based ReID model and the camera network topology $\mathbf{G} = (\mathbf{V}, \mathbf{E})$. For the appearance-based ReID model, we trained FastReID [11] to extract the appearance similarity. ResNet-50 [10] is set to its backbone network structure and the training parameters are as follows: epoch – 60, batch size – 64. Note that we can use other state-of-the-art appearance-based ReID models for our framework. The estimated camera network topology consists of 400 object transition time distributions (p_{ij}). Among them, 380 distributions are between different camera pairs (i.e., p_{ij} , where $c_i \neq c_j$), and the other 20 distributions are the distributions between themselves (i.e., p_{ij} , where $c_i = c_j$). Each distribution has 300 bins, and a bin covers 100 frame ranges. All the distributions were estimated based on the proposed adaptive Parzen window.

The proposed fusion network (fusionNet) has a single hidden layer, and we designed the number of nodes in the hidden layer to be around 65% of the size of the input vector by $\text{round}(2(2W + 2)/3 + 1)$. The training parameters of the network are as follows: epoch – 100, batch size – 128, learning rate – 0.001, optimizer – Adam. To train fusionNet and evaluate the ReID performance, we utilized 1,678 query images and 11,579 gallery images from 200 vehicle iden-

Methods	Rank-1	Rank-5	mAP
<i>Only appearance</i> [11]	96.96	98.45	81.91
<i>Without fusionNet</i> [35]	95.77	97.74	85.47
fusionNet ($W = 0$)	98.21	99.70	89.66
fusionNet ($W = 2$)	99.17	99.76	92.42
fusionNet ($W = 4$)	99.23	99.70	91.83
fusionNet ($W = 6$)	99.40	99.64	92.70
fusionNet ($W = 8$)	99.34	99.70	92.47
fusionNet ($W = 10$)	99.64	99.82	92.79
fusionNet ($W = 12$)	99.46	99.82	92.76

Table 1. ReID performances according to W values in fusionNet. The method *Only appearance* does not exploit spatial-temporal information S_T . The method *without fusionNet* estimates the final similarity by $S_F = S_A(\mathbf{I}_i^m, \mathbf{I}_j^n) \cdot p_{ij}(\tau_{ij}^{mn})$ as in [35].

ties. For fair comparison, a 5-fold cross-validation was conducted, and we evaluated Top- k accuracy ($k = 1, 5$) and mean Average Precision (mAP) scores.

5.2. Effects of fusionNet

The proposed fusionNet that combines appearance similarity S_A and spatial-temporal distributions S_T can improve the ReID performance. To compare the performance, we also evaluated two baseline methods (1. *Only appearance*, 2. *Without fusionNet*). *Only appearance* based on FastReID [11] performed ReID only using appearance similarities (S_A) between images. Another baseline *Without fusionNet* estimated appearance similarity (S_A) by FastReID [11] and simply combined spatial-temporal similarity by $S_F = S_A(\mathbf{I}_i^m, \mathbf{I}_j^n) \cdot p_{ij}(\tau_{ij}^{mn})$ as in [35]. For the fusionNet, we tested various W values to determine the spatial-temporal vector S_T .

As shown in Table 1, the appearance-based ReID [11] achieved rank-1 accuracy of 96.96% and 81.91% of mAP score. That is quite high performance in vehicle ReID, but there is still room for improvement. Using additional spatial-temporal similarity without fusionNet, it could improve the mAP score of appearance-based ReID [11] by 3.56%. However, combining strategy of two different similarities $S_A(\mathbf{I}_i^m, \mathbf{I}_j^n), p_{ij}(\tau_{ij}^{mn})$ is not optimized yet. Rank-1 and rank-5 performances were rather degraded after using spatial-temporal information.

Based on the proposed fusionNet, we can further improve the vehicle ReID performance. When the W was set to 10, fusionNet achieved the best performance by rank-1 accuracy of 99.64%, rank-5 accuracy of 99.82% and 92.79% of mAP score. Except for $W = 0$, fusionNet outperformed other methods in both evaluation metrics (rank-1, -5, mAP). This result supports that the proposed fusionNet can optimally combine different types of information such as appearance similarity and spatial-temporal information.

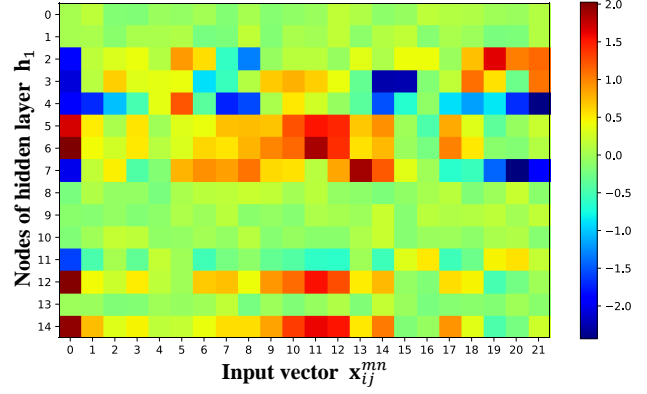


Figure 4. A visualization of the trained weight vector (\mathbf{w}_1) between input and hidden layer (\mathbf{h}_1)

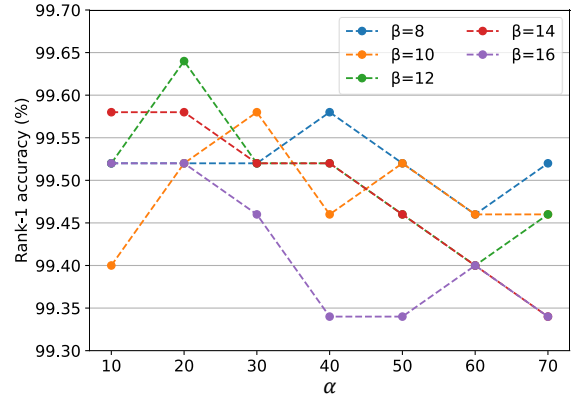


Figure 5. Performances according to factors α and β of the adaptive Parzen window

Figure 4 shows a visualization of the trained weight vector (\mathbf{w}_1) between input and hidden layer (\mathbf{h}_1). The row numbers (0–14) denote the index of the nodes in \mathbf{h}_1 , and column numbers (0–22) denote the index of the input vector \mathbf{x}_{ij}^{mn} . The first column (0 index) shows the weights for appearance similarity (S_A). As we can see, the magnitudes of the weights are relatively bigger than those of other weights. It means that the fusion network properly trained the importance of the appearance similarity (S_A). The other columns (from 0 to 21 index) are the weights for spatial-temporal distribution (S_T). Interestingly, the weights from the 10th to 12th columns showed large magnitudes. It implies that the spatial-temporal information around the time difference (τ_{ij}^{mn}) between two images plays a key role in ReID.

5.3. Effects of adaptive Parzen window

For the proposed adaptive Parzen window method, we tested various factors such as a scale factor α and smoothness factor β in Eq. 4. In all experiments, we set $W = 10$

Methods	Rank-1	Rank-5	mAP
fixed $\sigma = 1$	99.46	99.70	92.79
fixed $\sigma = 10$	99.52	99.82	92.61
fixed $\sigma = 100$	99.52	99.82	89.97
fixed $\sigma = 300$	99.17	99.70	87.98
(Ours) adaptive σ	99.64	99.82	92.79

Table 2. ReID performances according to the values of σ for Parzen window method

for the fusionNet. Figure 5 illustrates rank-1 performances according to the factors α and β . When the scale factor $\alpha = 20$ and the smoothness factor $\beta = 12$, the proposed framework achieved the best performance at rank-1 accuracy. Note that the rank-1 performance does not fluctuate significantly due to the factor values (min: 99.34, max: 99.64).

We then compared ReID performances of the fixed σ and adaptive σ . We tested the fixed σ by 1, 10, and 300, and the adaptive σ as in Eq. 2 as shown in Table 2. The fixed $\sigma = 300$ showed the lowest performance, because too large σ leads smoothed distributions that is close to uniform distribution, and reduces the impact of spatial-temporary information. $\sigma = 1$ and $\sigma = 10$ performed relatively well, achieving higher than 99% rank-1 accuracy. Compared to using fixed σ values, the proposed adaptive Parzen window with the adaptive σ achieved the best performance in both evaluation metrics by the 99.64% rank-1 accuracy, 99.82% rank-5 accuracy and 92.79% mAP score. As we explained in Sec. 4.1 and Fig 3, a fixed value of σ is hard to handle the various types of initial histograms h_{ij} . This result implies that setting different σ_{ij} values by considering the different connection strengths of camera pairs is effective and improves the ReID performance.

5.4. Comparison with state-of-the-art methods

In this section, we compare the proposed method with state-of-the-art re-identification methods using a VeRi776 [23] vehicle ReID dataset. The methods are mainly categorized into two approaches: 1) only appearance-based, 2) using additional spatial-temporal information (marked by †). The methods marked by * performed re-ranking post-processing for final ReID results. Vehicle ReID results are summarized in Table. 3, and the list is sorted by rank-1 performance.

Compared to appearance-based approaches, fewer spatial-temporal approaches have been proposed. Although the spatial-temporal approaches [23, 24, 31] have improved their baseline methods, the performances are relatively low than other state-of-the-art methods. That is because their appearance models were slightly old-fashioned methods such as SIFT, Bag-of-words, and Siamese-CNN for ReID. Furthermore, the methods did not provide a direct estima-

Models	Rank-1	Rank-5	mAP
†FACT+Plate-SNN+STR [23]	61.44	78.78	27.77
†Siamese-CNN+Path-LSTM [31]	83.49	90.04	58.27
†PROVID [24]	81.56	95.11	53.42
†KPGST [16]	92.35	93.92	68.73
†FastReID [11] + Wang’s [35]	95.77	97.74	85.47
*GAN+LSRO [36]	88.62	94.52	64.78
*AAVER [19]	90.17	94.34	66.35
PAMTRI [34]	92.86	96.97	71.88
SPAN [4]	94.00	97.60	68.90
CAL [28]	95.40	97.90	74.30
PVEN [26]	95.60	98.40	79.50
TBE [33]	96.00	98.50	79.50
TransReID [13]	96.90	-	80.60
*VehicleNet [38]	96.78	-	83.41
*SAVER [20]	96.90	97.70	82.00
*DMT [12]	96.90	-	82.00
FastReID [11]	96.96	98.45	81.91
CLIP-ReID [22]	97.30	-	84.50
*Strong Baseline [17]	97.00	-	87.10
*RPTM [9]	97.30	98.40	88.00
Ours	99.64	99.82	92.79

Table 3. Performance comparisons on VeRi776 [23] data. †, * denote spatial-temporal approach and re-ranking, respectively.

tion of the camera network topology, nor did they optimize the utilization of spatial-temporal information. For the fair comparison, we implemented a spatial-temporal vehicle ReID model (*Without fusionNet*) by combining the methods FastReID [11] and Wang’s [35] as we explained in Sec. 5.2. Although it has the same appearance-based model as our method, our rank1 performance is 3.87% better.

As the deep learning model developments, many appearance-based methods have improved ReID performances without spatial-temporal information. For example, FastReID [11] which is our baseline appearance model achieved 96.96% rank-1 accuracy and 81.91% mAP score. Especially, RPTM [9] used GMS [3] feature matcher and employed ResNet-101 [10] structure showed the best performance by 97.30% of rank-1 accuracy, 88.00% of mAP score. Although our method used lightweight structure (ResNet-50) for the appearance model, we outperformed rank-1 accuracy of 2.34%, rank-5 accuracy of 1.37% and mAP score of 4.79% over the best score achieved by SOTA methods. In addition, the proposed method did not perform any re-ranking processes for the post-processing.

Figure. 6 illustrates qualitative vehicle ReID results. We compared our method with a baseline method (FastReID [11]) which used only appearance information. The baseline method occurs numerous false matches, where the appearances closely resemble that of the query image. In

Query ID	Model	Query	Rank-1	Rank-2	Rank-3	Rank-4	Rank-5	Rank-6	Rank-7	Rank-8	Rank-9	Rank-10
ID 30	Baseline											
	Ours											
ID 150	Baseline											
	Ours											
ID 662	Baseline											
	Ours											

Figure 6. Qualitative vehicle ReID results of baseline method and ours. The baseline method [11] is an appearance-based method. Green and red boxes denote the true and false matching, respectively. Compared to baseline method, the proposed method perfectly matches the true positive pairs despite of similar appearances. Best viewed in color.

particular, the baseline model rarely matched correct images of the 662-th query image due to many similar cars. On the other hand, our method perfectly matched correct images at rank-1 to rank-10 under those challenging query and gallery pairs. These results support that the proposed spatial-temporal vehicle ReID with fusionNet can effectively handle the appearance ambiguity problems, and overcome the limitations of the previous ReID methods. It is worth highlighting that the proposed vehicle ReID is simple but effective. Furthermore, it has high compatibility with various baseline models.

6. Conclusion

In this work, we proposed a vehicle ReID framework that can estimate camera network topology and combines appearance and spatial-temporal similarities to alleviate appearance ambiguities. To this end, we proposed an adaptive Parzen window for reliable topology estimation and a fusion network (fusionNet) for optimal similarity aggregation. The

proposed framework achieved superior performance for vehicle ReID with the rank-1 accuracy of 99.64% and mAP score of 92.79% on VeRi776 data. The results support that utilizing spatial and temporal information for ReID can leverage the accuracy of appearance-based methods and effectively deal with appearance ambiguities.

We confirmed the potential for the proposed framework and there are a few areas that could be explored for future work. First, we will utilize another appearance-based method as the baseline of the framework. Since satisfying results have been obtained by the most common baseline (ResNet structure with triplet loss optimization), we expect that our framework can improve other baselines as well. Second, we will extend our framework to other domains such as person ReID.

References

- [1] Ejaz Ahmed, Michael Jones, and Tim K Marks. An improved deep learning architecture for person re-identification. In

- Proceedings of the IEEE conference on computer vision and pattern recognition*, pages 3908–3916, 2015. 1, 2
- [2] Yan Bai, Yihang Lou, Feng Gao, Shiqi Wang, Yuwei Wu, and Ling-Yu Duan. Group-sensitive triplet embedding for vehicle reidentification. *IEEE Transactions on Multimedia*, 20(9):2385–2399, 2018. 2
- [3] JiaWang Bian, Wen-Yan Lin, Yasuyuki Matsushita, Sai-Kit Yeung, Tan-Dat Nguyen, and Ming-Ming Cheng. Gms: Grid-based motion statistics for fast, ultra-robust feature correspondence. In *Proceedings of the IEEE conference on computer vision and pattern recognition*, pages 4181–4190, 2017. 7
- [4] Tsai-Shien Chen, Chih-Ting Liu, Chih-Wei Wu, and Shao-Yi Chien. Orientation-aware vehicle re-identification with semantics-guided part attention network. In *Computer Vision–ECCV 2020: 16th European Conference, Glasgow, UK, August 23–28, 2020, Proceedings, Part II 16*, pages 330–346. Springer, 2020. 7
- [5] Yanbei Chen, Xiatian Zhu, and Shaogang Gong. Person re-identification by deep learning multi-scale representations. In *Proceedings of the IEEE international conference on computer vision workshops*, pages 2590–2600, 2017. 1, 2
- [6] De Cheng, Yihong Gong, Sanping Zhou, Jinjun Wang, and Nanning Zheng. Person re-identification by multi-channel parts-based cnn with improved triplet loss function. In *Proceedings of the IEEE conference on computer vision and pattern recognition*, pages 1335–1344, 2016. 2
- [7] Yeong-Jun Cho, Su-A Kim, Jae-Han Park, Kyuewang Lee, and Kuk-Jin Yoon. Joint person re-identification and camera network topology inference in multiple cameras. *Computer Vision and Image Understanding*, 180:34–46, 2019. 2, 3, 4, 5
- [8] Yeong-Jun Cho and Kuk-Jin Yoon. Improving person re-identification via pose-aware multi-shot matching. In *Proceedings of the IEEE conference on computer vision and pattern recognition*, pages 1354–1362, 2016. 2
- [9] Adhiraj Ghosh, Kuruparan Shanmugalingam, and Wen-Yan Lin. Relation preserving triplet mining for stabilising the triplet loss in re-identification systems. In *Proceedings of the IEEE/CVF Winter Conference on Applications of Computer Vision*, pages 4840–4849, 2023. 1, 2, 7
- [10] Kaiming He, Xiangyu Zhang, Shaoqing Ren, and Jian Sun. Deep residual learning for image recognition. In *Proceedings of the IEEE conference on computer vision and pattern recognition*, pages 770–778, 2016. 5, 7
- [11] Lingxiao He, Xingyu Liao, Wu Liu, Xinchun Liu, Peng Cheng, and Tao Mei. Fastreid: A pytorch toolbox for general instance re-identification. *arXiv preprint arXiv:2006.02631*, 2020. 1, 2, 5, 6, 7, 8
- [12] Shuting He, Hao Luo, Weihua Chen, Miao Zhang, Yuqi Zhang, Fan Wang, Hao Li, and Wei Jiang. Multi-domain learning and identity mining for vehicle re-identification. In *Proceedings of the IEEE/CVF Conference on Computer Vision and Pattern Recognition Workshops*, pages 582–583, 2020. 7
- [13] Shuting He, Hao Luo, Pichao Wang, Fan Wang, Hao Li, and Wei Jiang. Transreid: Transformer-based object re-identification. In *Proceedings of the IEEE/CVF international conference on computer vision*, pages 15013–15022, 2021. 2, 7
- [14] Alexander Hermans, Lucas Beyer, and Bastian Leibe. In defense of the triplet loss for person re-identification. *arXiv preprint arXiv:1703.07737*, 2017. 2
- [15] Wenxin Huang, Ruimin Hu, Chao Liang, Yi Yu, Zheng Wang, Xian Zhong, and Chunjie Zhang. Camera network based person re-identification by leveraging spatial-temporal constraint and multiple cameras relations. In *MultiMedia Modeling: 22nd International Conference, MMM 2016, Miami, FL, USA, January 4–6, 2016, Proceedings, Part I 22*, pages 174–186. Springer, 2016. 2
- [16] Wenxin Huang, Xian Zhong, Xuemei Jia, Wenxuan Liu, Meng Feng, Zheng Wang, and Shin’ichi Satoh. Vehicle re-identification with spatio-temporal model leveraging by pose view embedding. *Electronics*, 11(9):1354, 2022. 3, 5, 7
- [17] Su V Huynh. A strong baseline for vehicle re-identification. In *Proceedings of the IEEE/CVF conference on computer vision and pattern recognition*, pages 4147–4154, 2021. 2, 7
- [18] Sameh Khamis, Cheng-Hao Kuo, Vivek K Singh, Vinay D Shet, and Larry S Davis. Joint learning for attribute-consistent person re-identification. In *Computer Vision–ECCV 2014 Workshops: Zurich, Switzerland, September 6–7 and 12, 2014, Proceedings, Part III 13*, pages 134–146. Springer, 2015. 2
- [19] Pirazh Khorramshahi, Amit Kumar, Neehar Peri, Sai Saketh Rambhatla, Jun-Cheng Chen, and Rama Chellappa. A dual-path model with adaptive attention for vehicle re-identification. In *Proceedings of the IEEE/CVF international conference on computer vision*, pages 6132–6141, 2019. 7
- [20] Pirazh Khorramshahi, Neehar Peri, Jun-cheng Chen, and Rama Chellappa. The devil is in the details: Self-supervised attention for vehicle re-identification. In *Computer Vision–ECCV 2020: 16th European Conference, Glasgow, UK, August 23–28, 2020, Proceedings, Part XIV 16*, pages 369–386. Springer, 2020. 7
- [21] Martin Koestinger, Martin Hirzer, Paul Wohlhart, Peter M Roth, and Horst Bischof. Large scale metric learning from equivalence constraints. In *2012 IEEE conference on computer vision and pattern recognition*, pages 2288–2295. IEEE, 2012. 1, 2
- [22] Siyuan Li, Li Sun, and Qingli Li. Clip-reid: Exploiting vision-language model for image re-identification without concrete text labels. In *Proceedings of the AAAI Conference on Artificial Intelligence*, volume 37, pages 1405–1413, 2023. 2, 7
- [23] Xinchun Liu, Wu Liu, Tao Mei, and Huadong Ma. A deep learning-based approach to progressive vehicle re-identification for urban surveillance. In *Computer Vision–ECCV 2016: 14th European Conference, Amsterdam, The Netherlands, October 11–14, 2016, Proceedings, Part II 14*, pages 869–884. Springer, 2016. 2, 3, 5, 7
- [24] Xinchun Liu, Wu Liu, Tao Mei, and Huadong Ma. Provid: Progressive and multimodal vehicle reidentification for large-scale urban surveillance. *IEEE Transactions on Multimedia*, 20(3):645–658, 2017. 3, 7
- [25] Kai Lv, Heming Du, Yunzhong Hou, Weijian Deng, Hao Sheng, Jianbin Jiao, and Liang Zheng. Vehicle re-

- identification with location and time stamps. In *CVPR workshops*, pages 399–406, 2019. 3
- [26] Dechao Meng, Liang Li, Xuejing Liu, Yadong Li, Shijie Yang, Zheng-Jun Zha, Xingyu Gao, Shuhui Wang, and Qingming Huang. Parsing-based view-aware embedding network for vehicle re-identification. In *Proceedings of the IEEE/CVF conference on computer vision and pattern recognition*, pages 7103–7112, 2020. 7
- [27] Jiaxu Miao, Yu Wu, Ping Liu, Yuhang Ding, and Yi Yang. Pose-guided feature alignment for occluded person re-identification. In *Proceedings of the IEEE/CVF international conference on computer vision*, pages 542–551, 2019. 2
- [28] Yongming Rao, Guangyi Chen, Jiwen Lu, and Jie Zhou. Counterfactual attention learning for fine-grained visual categorization and re-identification. In *Proceedings of the IEEE/CVF International Conference on Computer Vision*, pages 1025–1034, 2021. 7
- [29] Min Ren, Lingxiao He, Xingyu Liao, Wu Liu, Yunlong Wang, and Tieniu Tan. Learning instance-level spatial-temporal patterns for person re-identification. In *Proceedings of the IEEE/CVF International Conference on Computer Vision*, pages 14930–14939, 2021. 3, 5
- [30] Leilei Rong, Yan Xu, Xiaolei Zhou, Lisi Han, Linghui Li, and Xuguang Pan. A vehicle re-identification framework based on the improved multi-branch feature fusion network. *Scientific Reports*, 11(1):20210, 2021. 2
- [31] Yantao Shen, Tong Xiao, Hongsheng Li, Shuai Yi, and Xiaogang Wang. Learning deep neural networks for vehicle re-id with visual-spatio-temporal path proposals. In *Proceedings of the IEEE international conference on computer vision*, pages 1900–1909, 2017. 2, 3, 7
- [32] Chi Su, Jianing Li, Shiliang Zhang, Junliang Xing, Wen Gao, and Qi Tian. Pose-driven deep convolutional model for person re-identification. In *Proceedings of the IEEE international conference on computer vision*, pages 3960–3969, 2017. 2
- [33] Wei Sun, Guangzhao Dai, Xiaorui Zhang, Xiaozheng He, and Xuan Chen. Tbe-net: A three-branch embedding network with part-aware ability and feature complementary learning for vehicle re-identification. *IEEE Transactions on Intelligent Transportation Systems*, 23(9):14557–14569, 2021. 7
- [34] Zheng Tang, Milind Naphade, Stan Birchfield, Jonathan Tremblay, William Hodge, Ratnesh Kumar, Shuo Wang, and Xiaodong Yang. Pamtri: Pose-aware multi-task learning for vehicle re-identification using highly randomized synthetic data. In *Proceedings of the IEEE/CVF International Conference on Computer Vision*, pages 211–220, 2019. 7
- [35] Guangcong Wang, Jianhuang Lai, Peigen Huang, and Xiaohua Xie. Spatial-temporal person re-identification. In *Proceedings of the AAAI conference on artificial intelligence*, volume 33, pages 8933–8940, 2019. 2, 3, 4, 5, 6, 7
- [36] Fangyu Wu, Shiyang Yan, Jeremy S Smith, and Bailing Zhang. Joint semi-supervised learning and re-ranking for vehicle re-identification. In *2018 24th International Conference on Pattern Recognition (ICPR)*, pages 278–283. IEEE, 2018. 7
- [37] Wei-Shi Zheng, Shaogang Gong, and Tao Xiang. Person re-identification by probabilistic relative distance comparison. In *CVPR 2011*, pages 649–656. IEEE, 2011. 1, 2
- [38] Zhedong Zheng, Tao Ruan, Yunchao Wei, Yi Yang, and Tao Mei. Vhiclenet: Learning robust visual representation for vehicle re-identification. *IEEE Transactions on Multimedia*, 23:2683–2693, 2020. 3, 7